Voroshilov, Pavel; Ovchinnikov, Victor; Papadimitratos, Alexios; Zakhidov, Anvar; Simovski, Constantin

Light Trapping Enhancement by Silver Nanoantennas in Organic Solar Cells

Published in:
ACS Photonics

DOI:
10.1021/acsphotonics.7b01459

Published: 10/04/2018

Document Version
Peer reviewed version

Please cite the original version:
Voroshilov, P., Ovchinnikov, V., Papadimitratos, A., Zakhidov, A., & Simovski, C. (2018). Light Trapping Enhancement by Silver Nanoantennas in Organic Solar Cells. *ACS Photonics*, *5*(5), 1767-1772. https://doi.org/10.1021/acsphotonics.7b01459

Light Trapping Enhancement by Silver Nanoantennas in Organic Solar Cells

Pavel M. Voroshilov,[*,†,‡] Victor Ovchinnikov,[‡] Alexios Papadimitratos,[¶] Anvar A. Zakhidov,[†,§,¶] and Constantin R. Simovski[†,‡]

†*ITMO University, Kronverkskiy pr. 49, 197101 St. Petersburg, Russia*
‡*Aalto University, P.O. Box 15500, 00076 Aalto, Finland*
¶*The University of Texas at Dallas, Richardson 75080, USA*
§*National University of Science and Technology MISiS, Moscow 119049, Russia*

E-mail: p.voroshilov@metalab.ifmo.ru

Abstract

In this paper, we study experimentally the enhancement of parameters of a typical organic thin film solar cell (OSC) achieved by an originally proposed light trapping structure (LTS). Our LTS is an array of silver nanoantennas supporting collective modes, what provide subwavelength light enhancement in the substrate. Low losses in the metal result from the advantageous optical field distribution that is achieved in the broad range of wavelengths. We study the enhancement of all the main photovoltaic (PV) parameters observed in OSC with our LTS, such as power conversion efficiency (PCE), which is effectively increased by 18%, fill factor (FF), that can also be effected positively and short-circuit current I_{sc} improvement. Although the Ag nanoantenna occupies up to 40% of the photoactive OSC area, it provides the nearly twice enhanced optical absorption, resulting in overall higher I_{sc} and FF. Improvements of the optical and electrical design of OSC architectures are discussed for further enhancement of performance.

Keywords

Metasurface, Nanoantennas, Small molecules, Organic solar cells, Light trapping, Dominomodes

The photovoltaic industry regularly requests new scientific and technical solutions for the successful global commercialization of renewable energy.[1] Considerable efforts have been made to enhance the efficiency of thin film solar cells which can find numerous applications (see e.g. in[1–4]). There is a variety of strategies to increase the efficiency of thin film solar cells, which include material development,[5,6] interface engineering,[7] improvements in fabrication and processing,[8] device architecture modernization[9] and optimization of charge transfer.[10]

Photon management by light-trapping nanostructures represents one of the promising ways to improve the performance of such solar cells, whose efficiency is limited due to insufficient absorption of light in the active (PV) layer. Absorption is limited by PV layer, which thickness lays in subwavelength range at frequencies of operation. Organic solar cells of exciton type (we do not refer dye-sensitized and perovskite solar cells as OSCs) have a fundamental limitation on the thickness of the PV layer – below 100-150 nm – due to small diffusion length of Frenkel's excitons.[11] Optical absorption of organic PV materials is also low. Therefore, the larger part of the incident sunlight passes through the PV layer. An anti-reflecting coating does not resolve the issue of low absorption.

Even if the thickness of the PV layer effectively doubled by a polished rear electrode it is insufficient. Moreover, many OSCs imply a transparent (conducting oxide) or absorbing (e.g. Al foil) rear electrode that does not completely reflect light back to the active layer. In this situation, one has to apply LTSs, usually performed as plasmonic nanostructures.[12]

In[13,14] we suggested a concept of light trapping employing a metasurface of metal nanoantennas, whose resonances cover a very broad band of wavelengths. These resonances correspond to collective oscillations that keep even for a perfectly conducting metal. The field is locally enhanced in the gaps between the metal elements and the losses in the metal are almost absent. Such advantageous distribution origins from leaky modes[15] supported by the metasurface suggested in.[13] We call them leaky domino-modes by analogy with guided domino-modes which initially were revealed in far-infrared[16] and visible[17] ranges for arrays of metal nanobars. Leaky domino-modes were studied theoretically in[15] and experimentally in.[18]

The aim of the present paper is to experimentally demonstrate the enhancement of a typical OSC by LTS with leaky domino-modes. Since the pioneering work by Ching W. Tang[19] on two-layer organic OSC based on a molecular donor-acceptor structure with a PCE of about 1%, the significant progress has been achieved in the improvement of OSC systems, leading to a PCE of over 11%[20] in single-junction and over 13%[21] in tandem small-molecule based devices with a polished rear electrode. However, the main drawback inherent to typical OSCs by C.W. Tang keeps – the absorption of light is insufficient even in these advanced OSCs. Therefore, high optical losses still determine the comparatively low efficiency of organic solar photovoltaics compared to silicon photovoltaics.

Usually, in papers on LTSs, the increase of optical absorption in the active layer is claimed as a sufficient evidence of the efficiency enhancement because it results in the corresponding increase of the short-circuit current I_{sc}.[22] However, the total PCE of a solar cell is affected not only by I_{sc} but also by other parameters such as FF and open circuit voltage V_{oc}:

$$PCE = \frac{V_{oc} \cdot I_{sc} \cdot FF}{P_{in}}, \qquad (1)$$

where P_{in} is the power of the incident light (referred to the surface of our thin film solar cell and integrated over the spectrum). In accordance with Eq. 1 an LTS in order to grant the enhancement must not harm both FF and V_{oc}, otherwise, the overall efficiency may decrease. In this paper, we study the effect of proposed LTS on all mentioned parameters. Our target is the enhancement of PCE.

An explicit example of an OSC that can be drastically improved by our LTS is a small-molecule OSC[14] operating in the near-infrared and transparent for the visible light. In that work, we have chosen a bulk-heterojunction small-molecule OSC with phthalocyanine as a donor and fullerene as an acceptor. We preferred this design as the typical one that is sufficiently simple in fabrication.

In our theoretical work,[14] we have shown that proposed LTS increased the absorption of infrared solar light in the tin phthalocyanine (SnPc, donor) – fullerene (C60, acceptor) layers of the OSC more than triple. That OSC had two indium tin oxide (ITO) electrodes (both anode and cathode), that made it transparent for visible light, though by a price of very low efficiency.[3] Our LTS with its triple enhancement of the useful absorption promises a nearly double increase of the short-circuit current and, perhaps, a twice higher PCE (though this question was not studied). Meanwhile, the transmittance of visible light is kept sufficient for the effective transparency of a window into which such the enhanced OSC could be incorporated.

For estimation of the effective increase of the short-circuit current, both proper optical and electrical simulations should be performed, as in has been done e.g. in.[23] It is not easy to predict how both optical absorption and photocurrent can be optimally improved simultaneously. So increased optical absorption (and number of photogenerated carriers) can be achieved by increasing photoactive layer thickness, however this may lead to overall decrease of the expected

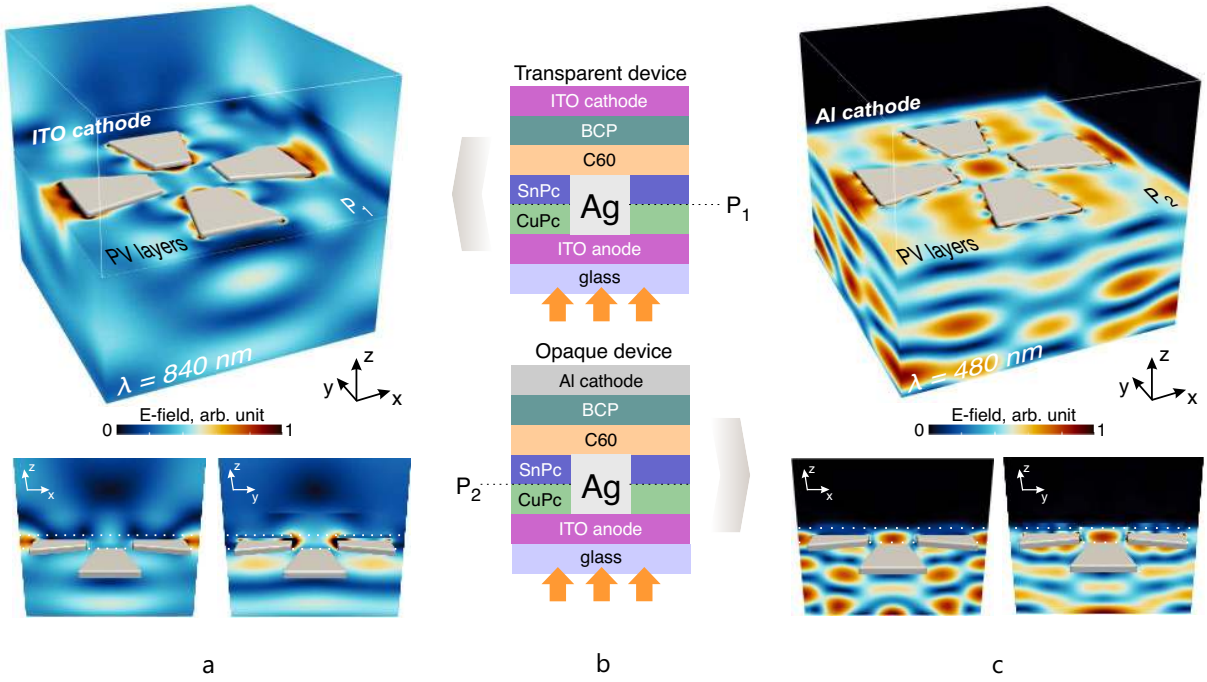

Figure 1: Normalized electric field intensity distributions in the horizontal planes P_1 and P_2 (top panel) and in the slightly tilted cross-sections (bottom panel) for an OSC containing ITO anode and cathode, λ =840 nm (a) and for a similar OSC with ITO anode and Al cathode, λ =480 nm (c). Active layer boundaries are shown as white dotted lines (bottom panel). Ag nanoantennas are located on top of ITO anode, embedded into the PV layer. In panel (b) we show the OSC schematics for these two cases. Horizontal planes P_1 and P_2 are shown as black dashed lines. Orange arrows show the wave incidence.

PCE enhancement due to poor charge collection from thicker layer (due to e.g. short diffusion length of carriers, and higher series resistance of thicker layer) and thus overall decreased fill factor. Therefore in future, we will qualitatively validate the numerical model of nanoantennas incorporated in a solar cell with the experimental results for further development of the efficient light-trapping concept for high PCE solar cells.

Unfortunately, in the present work, we did not manage to fabricate a transparent ITO cathode. Therefore, the experimental realization of the exactly same structure as in[14] turned out to be impossible. We have replaced ITO for the cathode by Al and dropping the functionality of the transparency concentrated on the effect of light trapping and its implications. Since in this case the transparency of the PV layer is not required, we have deviated from the design of[14] adding a nanolayer of copper phthalocyanine (CuPc) as an additional donor and hole transport layer (HTL). It allowed us to create a double heterojunction and to increase the initial efficiency of the prototype. Our new design is typical and corresponds to works.[9,11] In order to demonstrate the advantageous operation of our LTS, we do not modify the design parameters of the prototype. In this meaning, our study fairly demonstrates the real enhancement granted by the LTS to a typical OSC.

The HTL of CuPc has maximal absorption in the visible region. Therefore, conversion of solar radiation occurs in the extended spectral range, which includes both the near infrared (750-900 nm) part where the absorbing material is SnPc and the visible part (550-750 nm), where CuPc absorbs. One more difference of the present design from that of[14] is the slight shift of the metasurface with respect to the ITO anode. Instead of embedding the nanoantennas into ITO, we locate them on the ITO surface that allowed us to strongly simplify the fabrication.

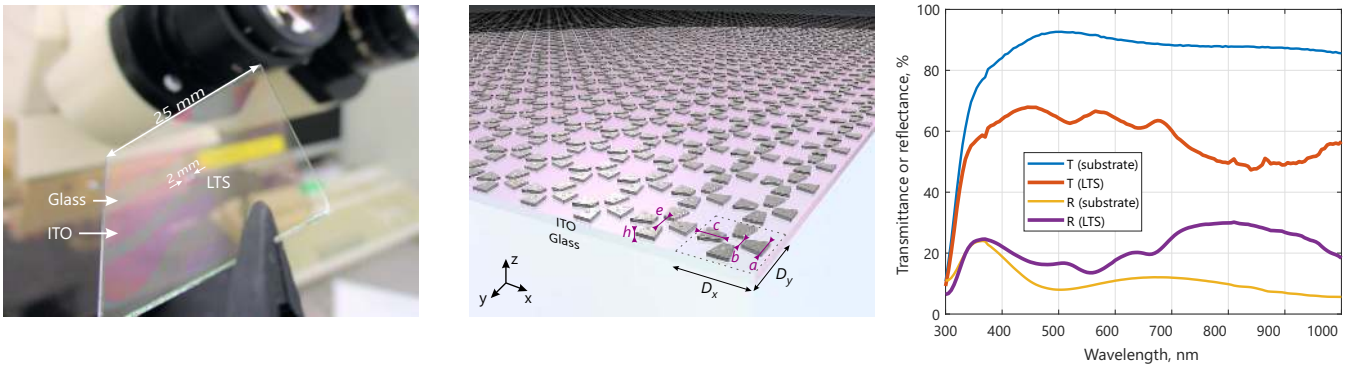

Figure 2: (a) Photo of the sample with our LTS. (b) Scheme of the metasurface geometry. The geometrical parameters are as follows: $D_x = D_y = 1000$ nm, $a = 300$ nm, $b = 150$ nm, $c = 300$ nm, $e = 250$ nm, $h = 35$ or 50 nm (two different samples). (c) Transmission and reflection spectra were measured for 50-nm sample (LTS) and for bare ITO area (substrate).

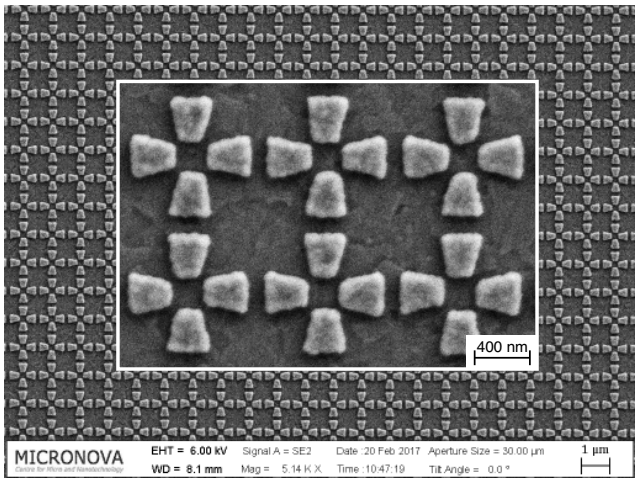

Figure 3: Scanning electron microscope image of our LTS.

Although the design modifications listed above may seem insignificant, they can drastically affect the performance of the LTS. It becomes necessary to study the influence of the Al cathode on the local electric field distribution inside the PV cell. We have performed full-wave (CST) electromagnetic simulations of two PV devices: one with a transparent ITO cathode and another with an opaque Al cathode. Complex refractive indexes were taken from.[24–26] Electric field intensity distributions for these two cases are presented in Fig. 1. Indeed, the opaque metal film fully changes the hot spots arrangement in the bulk of the structure at all wavelengths. Obviously, in presence of a transparent cathode, an effective Fabry-Perot cavity is formed in the structure that works together with domino-modes excited in our nanoantennas and leads to the more advantageous location of hot spots in the near-infrared range (700-850 nm). Meanwhile, in this configuration, these spots do not appear at other wavelengths. The situation changes when Al replaces ITO as a cathode material: hot spots now also appear in the visible range exactly in favorable locations. However, in the near-infrared band hot spots shift away from the PV layer. Anyway, this does not result in noticeable parasitic losses because these hot spots do not intersect with the metal. In general, simulations confirmed our expectations – the enhancement of the useful absorption keeps after the replacement of ITO by an aluminum. More details on this modeling can be found in the Supporting information.

We have prepared two samples with 50 nm and 35 nm thick Ag nanoantennas on top of the ITO-glass substrate. These samples contain $1.5 \cdot 10^6$ and $3 \cdot 10^6$ unit cells of our LTS, respectively. Fabrication was done using electron-beam lithography (EBL) and electron-beam evaporation (see Methods and Supporting information). SEM analysis showed a very high quality of our nanoantenna arrays, as can be guessed from Figs. 2 and 3. We measured transmittance T and reflectance R for a 50-nm thick LTS (incidence from the glass side) and compared them with those obtained for the bare

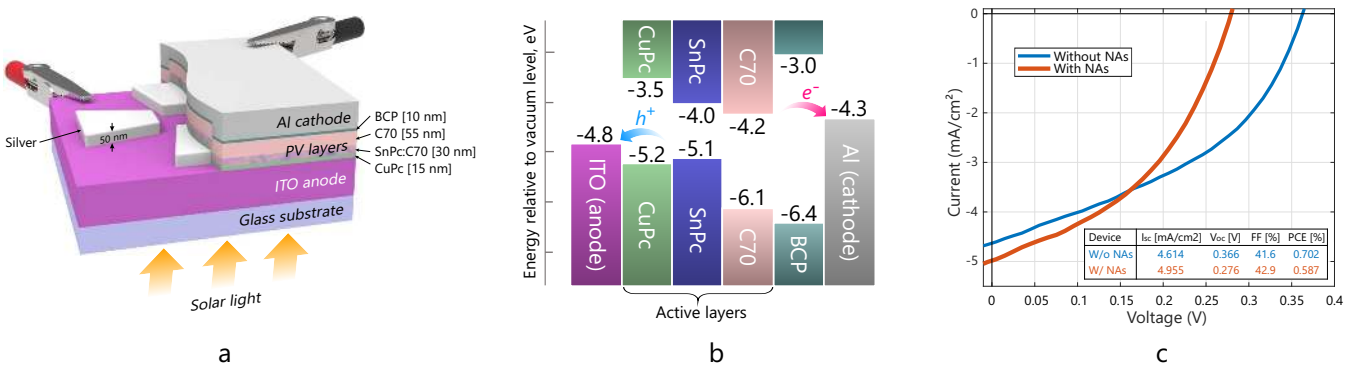

Figure 4: (a) Cross-section schematics of the OSC with C70 as an acceptor layer and 50-nm thick silver nanoantennas. (b) Energy-level band diagram for the current configuration. (c) IV curves measured under illumination for two cases: with (red line) and without (blue line) nanoantennas.

substrate (glass and ITO). The result is shown in Fig. 2 (c). The averaged reflectance growth is about 10%. Notice, that this negative effect keeps for the OSC, where it is overcompensated by the light-trapping effect.

The target of these simulations is twofold. Firstly, we may estimate the increase of the parasitic absorption A introduced by our LTS. Since the losses in Ag elements are negligibly small, parasitic absorption can be attributed to optical losses in ITO. From energy balance, we have $A = 1 - R - T$. For integral absorption in the operational range λ =400-900 nm we have nearly 5% in absence of our LTS and nearly 8% in its presence. This is an acceptable harm. Secondly, we may see that the reflectance grows much less that it can be estimated using the geometrical optics. Really, Ag nanoantennas cover almost 40% of the area, but the reflectance is λ-dependent and much lower than 0.4. This is so because the eigenmodes of our LTS are excited by the normally incident plane wave, what makes geometrical optics inadequate.

Further, inspecting the opaque design depicted in Fig. 1 we decided to additionally fabricate a variant of the OSC with C70 fullerene derivative instead of C60. If the impact of our LTS will be more significant for the structure with C70, it will confirm the shift of light-trapping regime (predicted by our simulations) from the IR range to the visible range for Al cathode. This should be so because C70 has higher absorption than C60 below λ =700 nm, whereas C60 has higher absorption at longer waves.

Our first sample with 50 nm-thick nanoantennas has the following structure above the glass substrate: ITO anode (150 nm) / CuPc (15 nm) / SnPc:C70 (30 nm) / C70 (55 nm) / BCP (10 nm) / Al (70 nm). The corresponding schematic is shown in Fig. 4 (a). This configuration with co-evaporated phthalocyanine and fullerene leads to the formation of two donor-acceptor heterojunctions: CuPc/C70 and SnPc/C70. We illuminated our sample with an AM 1.5G solar simulator from the side of glass through a 1 mm aperture. We measured the IV dependencies of our sample illuminating either the 1 mm areas comprising our nanoantennas or 1 mm areas free of them. In this way, we have collected sufficient statistics for a reliable plotting two IV-curves – one for an OSC enhanced by our LTS and another for a bare OSC (with only antireflective coating). These curves are shown in Fig. 4 and demonstrate a noticeable increase of I_{sc} caused by our LTS. Photocurrent generated in the nanoantenna area reaches the value 5 mA/cm^2, whereas the structure without nanoantennas gives 4.6 mA/cm^2. This 8% increase of the photocurrent corresponds to a higher increase of the PV absorbance due to a nonlinear current response of such OSC.[27]

Due to 40% of the area covered by Ag nanoantennas, the photoactive area that photogenerates carriers and provides I_{sc} is only 60% of the similar area in a reference OSC. Therefore the

actual enhancement of I_{sc}, provided by the LTS is not 5 mA/cm^2, but 5/0.6 = 8.3 mA/cm^2. The Ag nanoantenna array occupied area is not creating carriers but is creating concentration and enhancement of the photonic electrical field which results in the nearly twice enhancement of the optical absorption of light, resulting in 8.3 mA / 4.6 mA = 1.8 times enhanced concentration of carriers. We assume here that the edges of sharp Ag structures do not provide better charges collection (since the nanoantennas can collect only electrons by low work function), but on the contrary, are creating leakage of carriers and quenching of excitons. Despite all those negative effects of Ag nanoantennas: shading the useful area, wrong work function, recombination of electrons and holes on Ag nanostructures, we have still observed the overall sizable enhancement of I_{sc} = 5 mA (8% more than in the reference cell) at a nearly twice small photoactive area.

Fill factor calculated from IV characteristics is improved by 2.6% for our LTS (see inset of Fig. 4 (c)). Unfortunately, the open-circuit voltage V_{oc} of the area with nanoantennas decreased by 0.09 V, i.e. 25% compared to the bare OSC. This harm overshadows the positive gain in photocurrent and negatively affects the overall PCE. The possible reason for the fall in V_{oc} could be quite substantial dimensions of metal nanoantennas compared with ultrathin active layers. Really, V_{oc} in OSCs is directly proportional to the difference between the Fermi levels, and the ITO electrode having the bandgap in the ultraviolet has an impact on V_{oc}. Silver elements having the ohmic contact with ITO may modify the effective bandgap of the electrode. As a result, the difference of the Fermi levels squeezes and V_{oc} becomes smaller.

Parameters of the OSC with nanoantennas and without nanoantennas are shown in the inset of Fig. 4 (c). These data are averaged over several sample areas, as explained above.

Our next example is totally identical to the previous one exclude replacement of C70 by C60 and thinner Ag elements (35 nm instead of 50 nm). The structure is shown in Fig. 5 (a). It consists of the following layers on the glass plate: ITO (150 nm) / CuPc (15 nm) / SnPc:C60 (30 nm) / C60 (25 nm) / BCP (10 nm) / Al (70 nm). Since C60 is less absorptive material in the visible range and its thickness decreased, the impact of our LTS in the photocurrent also decreased compared to the previous case – 4.6% instead of 8%, as can be seen from Fig. 5 (c). However, thinner metal elements improved FF by 19% versus 2.6%, whereas V_{oc} almost kept unchanged. Total averaged value of the PCE enhancement is 18% that is a quite competitive result and is higher than the gain provided by known plasmonic counterparts of our LTS for similar OSCs (see e.g.[28]).

It should also be noted, that our samples were not encapsulated. Therefore, in order to prevent the degradation of organic materials and oxidation of Ag, our measurements were performed at room temperature and in an inert atmosphere. In order to prevent Ag nanoantennas tarnishing during transportation from the clean room to the laboratory, where the solar cell was prepared, we used a polymer protective coating. This coating was removed in the laboratory with acetone. However, all samples were treated by gentle UV-ozone for additional cleaning before the organic layer deposition.[29] So, a certain oxidation of the thin silver elements might take place during this treatment. This is another reason, why the increase of the PV absorption granted by our LTS in reality turned out to be lower than that predicted by numerical simulations. Hopefully, the experimental enhancement offered by our nanoantennas will increase once more, if the fabrication facilities will allow lithography process and solar cell preparation in the same clean room.

To summarize, in this paper, we have theoretically and experimentally proved that our original LTS from silver nanoantennas can sufficiently increase the efficiency of OSCs. First of all, our numerical simulations have shown advantageous field distributions that predicted enhancement of the useful absorption. Secondly, we have fabricated several OSCs with different materials and measured gain in PV parameters caused by nanostructures. Since total PCE of a solar cell is affected not only by I_{sc}, but also by fill factor FF and open circuit voltage (V_{oc}),

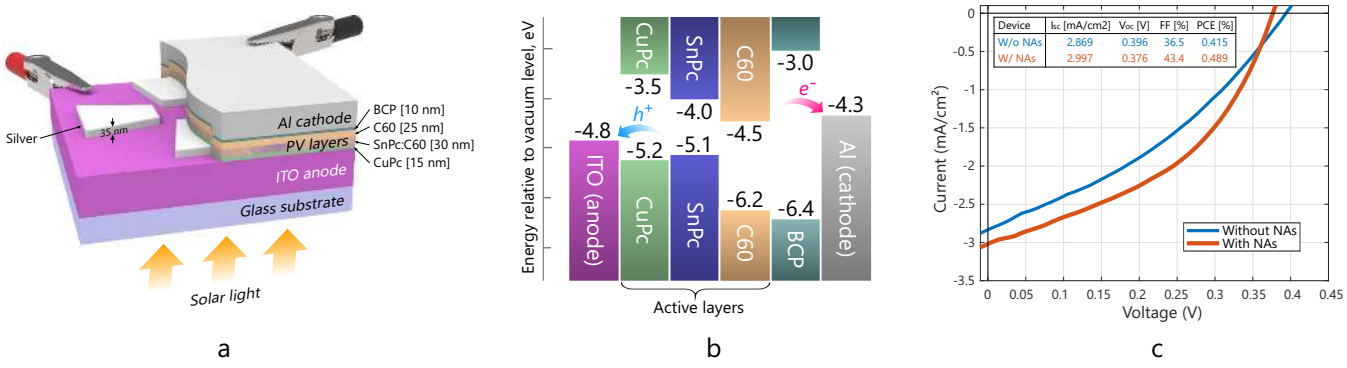

a b c

Figure 5: (a) Cross-section schematics of the OSC with C60 as an acceptor layer and 35-nm thick silver nanoantennas. (b) Energy-level band diagram for the current configuration. (c) IV curves measured under illumination for two cases: with (red line) and without (blue line) nanoantennas.

we have considered several design solutions and discussed the influence of the device architecture on LTS performance. Experimental data for our OSCs based on C60 fullerene and enhanced by 35 nm thick nanoantennas show the enhancement 18% that qualitatively fits the results of simulations. Other experimental data are also in line with theoretical expectations. We believe that the present results are helpful for further development of LTSs for thin film solar cells. In our future designs, we will choose nanoantennas with proper work function contributing into collection of holes at ITO side and with better location allowing us to avoid the 40% shading of the PV layer.

Methods

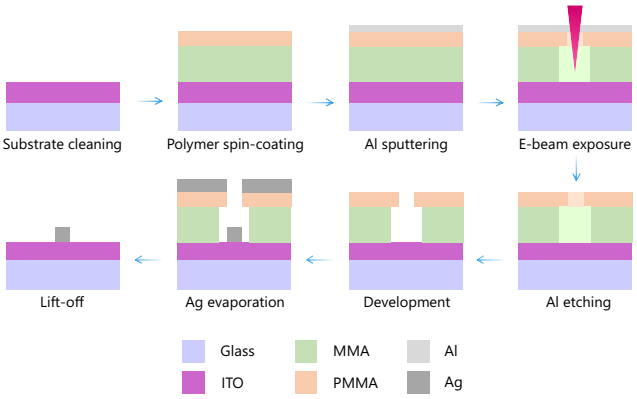

Figure 6: Process flow diagram illustrating fabrication steps of LTS.

Several samples with silver nanoantennas were fabricated on top of 150 nm-thick ITO coated glass substrates purchased from Luminescence Technology Corp by EBL and lift-off process in the Micronova Nanofabrication Centre of Aalto University. Process flow diagram is shown in Fig. 6. Substrates were preliminary cleaned with acetone and isopropanol (IPA) in an ultrasonic bath at 40° C and rinsed in DI-water. A copolymer resist (MMA) with concentration of solids 11% in Ethyl Lactate and polymer resist (950PMMA A) with concentrations of solids 2.25% in Anisole (both from Microchem) were sequentially deposited by spin-coating. Samples were dried on a hot plate for 3 minutes at a temperature of 160 degrees after each spin-coating procedure resulting in formation of 400 and 100 nm layers of MMA and PMMA, respectively. A thin (20 nm) sacrificial layer of aluminum was sputtered. The purpose of this layer is to solve the problem with e-beam focusing on a dielectric layer during EBL. E-beam exposure was done using Vistec EBPG 5000Plus ES tool at 100 keV with 4 nA current beam and 1000 μC/cm^2 e-beam dose. Then, samples were processed in etching mixture PWS 80-16-4 (65) from Honeywell containing phosphoric acid and nitric acid to completely remove the sacrificial aluminum layer. Next, PMMA and MMA were developed in solution of 1:3 MIBK:IPA during 30 sec and then rinsed in IPA during 30 sec to terminate development and prevent scumming. Silver was deposited by using electron beam evaporation at a rate of 2 Å/s and operating pressure of 10^{-7} mbar. Finally, non-exposed areas of poly-

mer layers were washed out together with silver on their surface by acetone in the ultrasonic bath. Samples were characterized by using AFM (DI3100), SEM (Zeiss Supra 40), and multifunctional tool for reflection (R), transmission (T) and quantum efficiency (QE) measurements (QEX10).

Small molecule OSCs were prepared in the multi-source high-vacuum system (Angstrom Engineering Inc., Canada) by sequential thermal evaporation onto ITO-glass substrates with our nanostructures of the following films: a 15 nm thick copper(II) phthalocyanine (from H.W. Sanders Corp) HTL, a 30 nm thick co-evaporated in equal quantity SnPc:fullerene mixed D:A layer, an additional continuous fullerene layer (25 or 55 nm), BCP (10 nm) and Al (70 nm) layers. We used C60 and C70 fullerenes (both >98% from Nano-C). Base pressure of the chamber was kept around 10^{-8} mbar during evaporation. Evaporation rate for separate layers was 0.5 Å/s, while co-evaporation rate was equal to 0.25 Å/s for each particular material. OSCs were characterized with an AM 1.5G solar simulator calibrated to one sun (100 mW/cm^2) through aperture holes of 1 mm in diameter, which provided selective illumination of nanostructured regions only.

Acknowledgement This work was partially supported by the Ministry of Education and Science of the Russian Federation (Grant 14.Y26.31.0010) and Nokia Foundation. The authors thank Mikhail Omelyanovich, Kristina Ianchenkova, and Matthias Meschke for useful discussions. We also acknowledge the provision of facilities and technical support by Aalto University at Micronova Nanofabrication Centre.

Supporting information

The Supporting Information (SI) is available free of charge on the ACS Publication website. The SI includes details of 3D electromagnetic modeling and additional simulated electric field distributions at different wavelengths. Moreover, the SI contains complementary SEM and AFM analysis of samples.

References

(1) Bosio, A.; Romeo, A. Thin Film Solar Cells: Current Status and Future Trends; Energy science, engineering and technology series; Nova Science Publishers, 2011.

(2) Schmidt-Mende, L.; Weickert, J. Organic and Hybrid Solar Cells: An Introduction; De Gruyter Textbook; De Gruyter, 2016.

(3) Lunt, R. R.; Bulovic, V. Transparent, near-infrared organic photovoltaic solar cells for window and energy-scavenging applications. Applied Physics Letters **2011**, 98, 61.

(4) Lipomi, D. J.; Bao, Z. Stretchable, elastic materials and devices for solar energy conversion. Energy & Environmental Science **2011**, 4, 3314–3328.

(5) Sun, S.-S.; Sariciftci, N. S. Organic photovoltaics: mechanisms, materials, and devices; CRC press, 2005.

(6) Brédas, J.-L.; Norton, J. E.; Cornil, J.; Coropceanu, V. Molecular understanding of organic solar cells: the challenges. Accounts of chemical research **2009**, 42, 1691–1699.

(7) Steim, R.; Kogler, F. R.; Brabec, C. J. Interface materials for organic solar cells. Journal of Materials Chemistry **2010**, 20, 2499–2512.

(8) Krebs, F. C. Fabrication and processing of polymer solar cells: a review of printing and coating techniques. Solar energy materials and solar cells **2009**, 93, 394–412.

(9) Heremans, P.; Cheyns, D.; Rand, B. P. Strategies for increasing the efficiency of heterojunction organic solar cells: material selection and device architecture. Accounts of chemical research **2009**, 42, 1740–1747.

(10) Deibel, C.; Strobel, T.; Dyakonov, V. Role of the charge transfer state in organic

donor–acceptor solar cells. Advanced Materials **2010**, 22, 4097–4111.

(11) Riede, M.; Mueller, T.; Tress, W.; Schueppel, R.; Leo, K. Small-molecule solar cells – status and perspectives. Nanotechnology **2008**, 19, 424001.

(12) Atwater, H. A.; Polman, A. Plasmonics for improved photovoltaic devices. Nature materials **2010**, 9, 205–213.

(13) Simovski, C.; Morits, D.; Voroshilov, P.; Guzhva, M.; Belov, P.; Kivshar, Y. Enhanced efficiency of light-trapping nanoantenna arrays for thin-film solar cells. Optics express **2013**, 21, A714–A725.

(14) Voroshilov, P. M.; Simovski, C. R.; Belov, P. A. Nanoantennas for enhanced light trapping in transparent organic solar cells. Journal of Modern Optics **2014**, 61, 1743–1748.

(15) Voroshilov, P. M.; Simovski, C. R. Leaky domino-modes in regular arrays of substantially thick metal nanostrips. Photonics and Nanostructures-Fundamentals and Applications **2016**, 20, 18–30.

(16) Martin-Cano, D.; Nesterov, M.; Fernandez-Dominguez, A.; Garcia-Vidal, F.; Martin-Moreno, L.; Moreno, E. Plasmons for subwavelength terahertz circuitry. Optics Express **2010**, 18, 754–764.

(17) Simovski, C.; Luukkonen, O. Tapered plasmonic waveguides with efficient and broadband field transmission. Optics Communications **2012**, 285, 3397–3402.

(18) Sinev, I. S.; Voroshilov, P. M.; Mukhin, I. S.; Denisyuk, A. I.; Guzhva, M. E.; Samusev, A. K.; Belov, P. A.; Simovski, C. R. Demonstration of unusual nanoantenna array modes through direct reconstruction of the near-field signal. Nanoscale **2015**, 7, 765–770.

(19) Tang, C. W. Two-layer organic photovoltaic cell. Applied Physics Letters **1986**, 48, 183–185.

(20) Deng, D.; Zhang, Y.; Zhang, J.; Wang, Z.; Zhu, L.; Fang, J.; Xia, B.; Wang, Z.; Lu, K.; Ma, W.; Wei, Z. Fluorination-enabled optimal morphology leads to over 11% efficiency for inverted small-molecule organic solar cells. Nature communications **2016**, 7, 13740.

(21) Heliatek sets new Organic Photovoltaic world record efficiency of 13.2%. 2016; `http://www.heliatek.com/en/press/press-releases/details/heliatek-sets-new-organic-photovoltaic-worl`

(22) Lasnier, F. Photovoltaic engineering handbook; CRC Press, 1990.

(23) Mirsafaei, M.; Fallahpour, A. H.; Lugli, P.; Rubahn, H.-G.; Adam, J.; Madsen, M. The influence of electrical effects on device performance of organic solar cells with nano-structured electrodes. Scientific reports **2017**, 7, 5300.

(24) O'Connor, B. Organic Electronics on Fibers for Energy Conversion Applications. Ph.D. thesis, University of Michigan, 2009.

(25) El-Nahass, M.; Yaghmour, S. Effect of annealing temperature on the optical properties of thermally evaporated tin phthalocyanine thin films. Applied Surface Science **2008**, 255, 1631 – 1636.

(26) Rand, B. P.; Li, J.; Xue, J.; Holmes, R. J.; Thompson, M. E.; Forrest, S. R. Organic Double-Heterostructure Photovoltaic Cells Employing Thick Tris (acetylacetonato) ruthenium (III) Exciton-Blocking Layers. Advanced Materials **2005**, 17, 2714–2718.

(27) Koster, L.; Mihailetchi, V.; Xie, H.; Blom, P. Origin of the light intensity dependence of the short-circuit current of polymer/fullerene solar cells. Applied Physics Letters **2005**, 87, 203502.

(28) Ahn, S.; Rourke, D.; Park, W. Plasmonic nanostructures for organic photovoltaic devices. Journal of Optics **2016**, 18, 033001.

(29) Chen, C.-W.; Hsieh, P.-Y.; Chiang, H.-H.; Lin, C.-L.; Wu, H.-M.; Wu, C.-C. Top-emitting organic light-emitting devices using surface-modified Ag anode. Applied physics letters **2003**, 83, 5127–5129.